Control and Cybernetics

vol. **34** (2005) No. 1

A regularized Newton method in electrical impedance tomography using shape Hessian information*

by

Karsten Eppler[1] and Helmut Harbrecht[2]

[1]Weierstraß Institut für Angewandte Analysis und Stochastik
Mohrenstr. 39, 10117 Berlin, Germany
e-mail: eppler@math.wias-berlin.de

[2]Institut für Informatik und Praktische Mathematik,
Christian–Albrechts–Universität zu Kiel
Olshausenstr. 40, 24098 Kiel, Germany
e-mail: hh@numerik.uni-kiel.de

Abstract: The present paper is concerned with the identification of an obstacle or void of different conductivity included in a two-dimensional domain by measurements of voltage and currents at the boundary. We employ a reformulation of the given identification problem as a shape optimization problem as proposed by Roche and Sokolowski (1996). It turns out that the shape Hessian degenerates at the given hole which gives a further hint on the ill-posedness of the problem. For numerical methods, we propose a preprocessing for detecting the barycentre and a crude approximation of the void or hole. Then, we resolve the shape of the hole by a regularized Newton method.

Keywords: electrical impedance tomography, shape optimization, boundary integral equation, Newton type descent.

1. Introduction

Let $D \subset \mathbb{R}^2$ denote a bounded domain with boundary $\partial D = \Sigma$ and assume the existence of a simply connected subdomain $S \subset D$, consisting of material with constant conductivity, essentially different from the likewise constant conductivity of the material in the annular subregion $\Omega = D \setminus \overline{S}$. We consider the identification problem of this inclusion if the Cauchy data of the electrical

*This research has been carried out when the second author stayed at the Department of Mathematics, University of Utrecht, The Netherlands, supported by the EU-IHP project *Nonlinear Approximation and Adaptivity: Breaking Complexity in Numerical Modelling and Data Representation.*

potential u are measured at the boundary Σ , i.e., if a single pair $f = u|_\Sigma$ and $g = (\partial u/\partial \mathbf{n})|_\Sigma$ is known.

The problem under consideration is a special case of the general conductivity reconstruction problem and is severely ill-posed. It has been intensively investigated as an inverse problem. We refer for example to Akduman and Kress (2002), Chapko and Kress (2003) and Hettlich and Rundell (1998) for numerical algorithms and to Friedmann and Isakov (1989) as well as Alessandrini, Isakov and Powell (1995) for particular results concerning uniqueness. Moreover, we refer to Brühl and Hanke (2000) and Brühl (2001) for methods using the complete Dirichlet–to–Neumann operator at the outer boundary. We emphasize that we focus in the present paper on exact measurements and do not consider noisy data.

Roche and Sokolowski (1996) introduced a formulation in terms of a shape optimization problem. Moreover, analysis and numerical results are presented for first order shape optimization algorithms. In the present paper we investigate the related second order methods, developed and applied by the authors in Eppler and Harbrecht (2003a, b, c, 2004b). Provided that the interface $\Gamma = \partial S$ is sufficiently regular, higher order smoothness for the objective can be shown by means of standard results. We assume the inclusion to be starshaped with respect to a given pole $\mathbf{x}_0 \in D$ and derive the second order shape derivatives in terms of polar coordinates. Furthermore, we prove compactness of the shape Hessian at the optimal domain $\Omega^\star = D\setminus\overline{S^\star}$. This degeneration implies exponential ill-posedness of the optimization problem and is of course strongly related to the known ill-posedness of the underlying identification problem. Consequently, it is essentially stronger then the degeneration in the illustrating example of Dambrine (2000) and is completely different from the regular coercive situations observed in Dambrine (2002), Eppler and Harbrecht (2004a). In particular, neither the validity of a sufficient second order condition nor quadratic convergence of the Newton method can be established.

Using finite Fourier series to represent the boundary of the inclusion we arrive at a finite dimensional optimization problem. This optimization problem will be minimized by a Newton method which has to be regularized due to its ill-posedness, i.e., due to the compactness of the shape Hessian at the optimal domain. Precisely, we employ a Tikhinov regularization for adjusting the search direction. By numerical experiments we show that our method outperforms first order algorithms. Introducing a preprocessing for detecting the barycentre and a first crude approximation of the inclusion, we are able to extend our approach also to the case of small inclusions without knowing the pole in advance. Concerning the further use of Newton method in shape optimization, we refer to Fujii and Goto (1990), Novruzi and Roche (1995) and Novruzi (1997). Using ideas from Eppler and Harbrecht (2003d), the authors recently extended the second order approach to three dimensions (Eppler and Harbrecht, 2004a).

The present paper is organized as follows. In Section 2 we present the physical model and reformulate the identification problem as a shape optimiza-

tion problem. We compute the gradient and the Hessian of the given shape functional. Then, in Section 3, we analyze the shape Hessian and prove its degeneration at the optimal domain. In Section 4 we discretize the boundary of the inclusion and replace the infinite dimensional optimization problem by finite dimensional one. Moreover, we propose a boundary element method to compute the shape functional as well as its gradient and Hessian. In Section 5, we perform several numerical experiments to compare the regularized Newton method with a quasi Newton method. In the last section, that is - Section 6, we state concluding remarks.

2. Shape problem formulation

2.1. The physical model

Let $D \in \mathbb{R}^2$ be a simply connected domain with boundary $\Sigma = \partial D$ and assume that an unknown simply connected inclusion S with regular boundary $\Gamma = \partial S$ is located inside the domain D satisfying $\operatorname{dist}(\Sigma, \Gamma) > 0$, see Fig. 1.

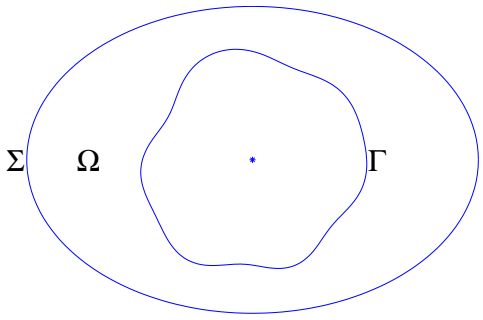

Figure 1. The domain Ω and its boundaries Γ and Σ

To determine the inclusion S we measure for a given current distribution $g \in H^{-1/2}(\Sigma)$ the voltage distribution $f \in H^{1/2}(\Sigma)$ at the boundary Σ. Hence, we are seeking a domain $\Omega := D \setminus \overline{S}$ and an associated harmonic function u, satisfying the system of equations

$$\begin{aligned} \Delta u &= 0 && \text{in } \Omega, \\ u &= 0 && \text{on } \Gamma, \\ u &= f && \text{on } \Sigma, \\ \frac{\partial u}{\partial \mathbf{n}} &= g && \text{on } \Sigma. \end{aligned}$$

This system denotes an overdetermined boundary value problem which admits a solution only for the true inclusion S.

Following Roche and Sokolowski (1996), we introduce the auxiliary harmonical functions v and w satisfying

$$\begin{aligned} \Delta v &= 0 \qquad \Delta w = 0 \qquad \text{in } \Omega, \\ v &= 0 \qquad w = 0 \qquad \text{on } \Gamma, \\ \frac{\partial v}{\partial \mathbf{n}} &= g \qquad w = f \qquad \text{on } \Sigma, \end{aligned} \tag{1}$$

and consider the following shape optimization problem

$$J(\Omega) = \int_\Omega \|\nabla(v-w)\|^2 d\mathbf{x} = \int_\Sigma \left(g - \frac{\partial w}{\partial \mathbf{n}} \right) (v-f) d\sigma \to \inf . \tag{2}$$

Herein, the infimum has to be taken over all domains including a void with sufficiently regular boundary. We refer to Roche and Sokolowski (1996) for the existence of optimal solutions with respect to this shape optimization problem.

2.2. Shape calculus

For the sake of clarity in presentation, we repeat the shape calculus concerning the problem under consideration by means of boundary variations. The shape gradient has been computed first in Roche and Sokolowski (1996), while the structure of the shape Hessian has been sketched in terms of material derivatives. But we emphasize that we derive a boundary integral representation of the shape Hessian which allows us to investigate and implement it. For a survey on the shape calculus based on the material derivative concept, we refer the reader to Sokolowski and Zolesio (1992) and Delfour and Zolesio (2001) and the references therein.

Let the underlying variation fields $\mathbf{V}$ be sufficiently smooth such that $C^{2,\alpha}$-regularity is preserved for all the perturbed domains. Moreover, for the sake of simplicity, we assume in addition that the outer boundary and the measurements are sufficiently regular such that the state functions $v = v(\Omega)$ and $w = w(\Omega)$ satisfy

$$v, w \in C^{2,\alpha}(\bar{\Omega}). \tag{3}$$

Then, a formal differentiation of (2) in terms of local derivatives yields immediately

$$dJ(\Omega)[\mathbf{V}] = \int_\Gamma \langle \mathbf{V}, \mathbf{n} \rangle \|\nabla(v-w)\|^2 d\sigma + 2 \int_\Omega \langle \nabla(v-w), \nabla(dv-dw) \rangle d\mathbf{x},$$

where the local shape derivatives $dv = dv[\mathbf{V}]$ and $dw = dw[\mathbf{V}]$ satisfy

$$\begin{aligned} \Delta dv &= 0 \qquad \Delta dw = 0 \qquad \text{in } \Omega, \\ dv &= -\langle \mathbf{V}, \mathbf{n} \rangle \frac{\partial v}{\partial \mathbf{n}} \qquad dw = -\langle \mathbf{V}, \mathbf{n} \rangle \frac{\partial w}{\partial \mathbf{n}} \qquad \text{on } \Gamma, \\ \frac{\partial dv}{\partial \mathbf{n}} &= 0 \qquad dw = 0 \qquad \text{on } \Sigma. \end{aligned} \tag{4}$$

Using $\partial\Omega = \Gamma \cup \Sigma$ and the known boundary data from (1) and (4), the boundary integral representation of the shape gradient is obtained via repeated integration by parts

$$dJ(\Omega)[\mathbf{V}] = \int_\Gamma \langle \mathbf{V}, \mathbf{n} \rangle \left[\left(\frac{\partial v}{\partial \mathbf{n}} \right)^2 - \left(\frac{\partial w}{\partial \mathbf{n}} \right)^2 \right] d\sigma, \tag{5}$$

see also Roche and Sokolowski (1996). Note that, as an immediate consequence of the shape calculus, (5) implies an simplified first order necessary condition

$$\frac{\partial v}{\partial \mathbf{n}} \equiv \frac{\partial w}{\partial \mathbf{n}} \quad \text{on } \Gamma. \tag{6}$$

In the case that the hole is starshaped S with respect to some pole $\mathbf{x}_0 \in D$, the boundary $\Gamma = \partial S$ can be parametrized by a function $r = r(\varphi)$ of the polar angle φ and the perturbation field $\mathbf{V}$ can be chosen as $\mathbf{V} = \mathbf{x}_0 + dr(\varphi)\mathbf{e}_r(\varphi)$. Herein, $\mathbf{e}_r(\varphi) := (\cos\varphi, \sin\varphi)^T$ denotes the radial direction with respect to the pole $\mathbf{x}_0$. The regularity requirements imply $r, dr \in C^{2,\alpha}_{\text{per}}[0, 2\pi]$, where r is a positive function such that $\text{dist}(\Sigma, \Gamma) > 0$ and

$$C^{2,\alpha}_{\text{per}}[0, 2\pi] := \{ r \in C^{2,\alpha}[0, 2\pi] : r^{(i)}(0) = r^{(i)}(2\pi),\ i = 0, 1, 2 \}.$$

Then, the shape gradient $dJ[dr]$ becomes

$$dJ(\Omega)[dr] = \int_0^{2\pi} dr(\varphi)\, r(\varphi) \left[\left(\frac{\partial w}{\partial \mathbf{n}} \right)^2 - \left(\frac{\partial v}{\partial \mathbf{n}} \right)^2 \right](\varphi)\, d\varphi, \tag{7}$$

where the minus sign results from the fact that $\langle \mathbf{e}_r, \mathbf{n} \rangle = -r/\sqrt{r^2 + r'^2}$.

To derive the shape Hessian, we proceed similarly to Eppler (2000a, b) by differentiating the shape gradient (7).

LEMMA 2.1 *The shape Hessian reads as*

$$\begin{aligned} d^2J(\Omega)[dr_1, dr_2] = \int_0^{2\pi} dr_1\, dr_2 \Bigg\{ & \frac{2rr'}{\sqrt{r^2 + r'^2}} \left[\frac{\partial v}{\partial \mathbf{n}} \frac{\partial^2 v}{\partial \mathbf{n} \partial \mathbf{t}} - \frac{\partial w}{\partial \mathbf{n}} \frac{\partial^2 w}{\partial \mathbf{n} \partial \mathbf{t}} \right] \\ & + \left(1 - \frac{2r^2\kappa}{\sqrt{r^2 + r'^2}} \right) \left[\left(\frac{\partial w}{\partial \mathbf{n}} \right)^2 - \left(\frac{\partial v}{\partial \mathbf{n}} \right)^2 \right] \Bigg\} \\ & + 2dr_1\, r \left\{ \frac{\partial w}{\partial \mathbf{n}} \frac{\partial dw[dr_2]}{\partial \mathbf{n}} - \frac{\partial v}{\partial \mathbf{n}} \frac{\partial dv[dr_2]}{\partial \mathbf{n}} \right\} d\varphi, \end{aligned} \tag{8}$$

where all data have to be understood as traces on the unknown boundary Γ.

Proof. We mention that our regularity assumptions provide the existence of a shape Hessian by means of standard theory, see Delfour and Zolesio (2001),

Sokolowski and Zolesio (1992). In particular, passing to the limit is always allowed and only briefly indicated in some of the following transformations. Moreover, we consider only the first part of the gradient, that is

$$dJ(\Omega)[dr] = \int_0^{2\pi} dr\, r \left(\frac{\partial w}{\partial \mathbf{n}}\right)^2 d\varphi,$$

since the second part is treated in complete analogy. We shall prove first the identity

$$d^2J(\Omega)[dr_1, dr_2] = \int_0^{2\pi} dr_1\, dr_2\, \|\nabla w\|^2 + dr_1\, dr_2\, r\, \frac{\partial}{\partial \mathbf{e}_r}\|\nabla w\|^2 + 2\, dr_1\, r\, \frac{\partial w}{\partial \mathbf{n}} \frac{\partial dw[dr_2]}{\partial \mathbf{n}} d\varphi\,. \tag{9}$$

The domain Ω respective boundary Γ can be identified with its parametrization, i.e., with the function $r : [0, 2\pi] \to \Gamma$. Similarly, we can identify the perturbed domain Ω_ε respective boundary Γ_ε with the function $r_\varepsilon = r + \varepsilon dr_2$. Therefore, we find

$$dJ(\Omega_\varepsilon)[dr_1] - dJ(\Omega)[dr_1] = \int_0^{2\pi} dr_1 \left\{ r_\varepsilon \left(\frac{\partial w_\varepsilon}{\partial \mathbf{n}_\varepsilon}\right)^2 - r \left(\frac{\partial w}{\partial \mathbf{n}}\right)^2 \right\} d\varphi,$$

where w_ε is the solution of the state equation with respect to the perturbed domain Ω_ε and $\mathbf{n}_\varepsilon$ is the outer normal of Ω_ε at Γ_ε. Inserting $r_\varepsilon = r + \varepsilon\, dr_2$ yields

$$dJ(\Omega_\varepsilon)[dr_1] - dJ(\Omega)[dr_1] = \int_0^{2\pi} \varepsilon\, dr_1\, dr_2 \left(\frac{\partial w_\varepsilon}{\partial \mathbf{n}_\varepsilon}\right)^2 d\varphi + \int_0^{2\pi} dr_1\, r \left\{ \left(\frac{\partial w_\varepsilon}{\partial \mathbf{n}_\varepsilon}\right)^2 - \left(\frac{\partial w}{\partial \mathbf{n}}\right)^2 \right\} d\varphi.$$

The first term in this expression will give the first term in (9). Hence, it remains to consider the difference

$$\left(\frac{\partial w_\varepsilon}{\partial \mathbf{n}_\varepsilon}\right)^2 - \left(\frac{\partial w}{\partial \mathbf{n}}\right)^2 = \langle \nabla w_\varepsilon\big|_{\Gamma_\varepsilon}, \nabla w_\varepsilon\big|_{\Gamma_\varepsilon}\rangle - \langle \nabla w\big|_{\Gamma}, \nabla w\big|_{\Gamma}\rangle.$$

By Taylor's expansion $r_\varepsilon^2 = r^2 + 2\varepsilon\, r\, dr_2 + \mathcal{O}(\varepsilon^2)$ we conclude

$$\langle \nabla w_\varepsilon\big|_{\Gamma_\varepsilon}, \nabla w_\varepsilon\big|_{\Gamma_\varepsilon}\rangle = \langle \nabla w_\varepsilon\big|_{\Gamma}, \nabla w_\varepsilon\big|_{\Gamma}\rangle + 2\varepsilon dr_2 \frac{\partial}{\partial \mathbf{e}_r} \langle \nabla w_\varepsilon\big|_{\Gamma_\xi}, \nabla w_\varepsilon\big|_{\Gamma_\xi}\rangle,$$

where Γ_ξ is defined via the radial function $r_\xi = r + \xi dr_2$, $0 < \xi < \varepsilon$. Inserting the local shape derivative $dw(\Omega)[dr]$ (4) we find

$$\nabla w_\varepsilon\big|_{\Gamma} = \nabla w\big|_{\Gamma} + \varepsilon dr_2 \nabla dw[dr_2]\big|_{\Gamma} + \mathcal{O}(\varepsilon^2),$$

and arrive at

$$\left(\frac{\partial w_\varepsilon}{\partial \mathbf{n}}\right)^2 - \left(\frac{\partial w}{\partial \mathbf{n}}\right)^2 = 2\varepsilon dr_2 \frac{\partial}{\partial \mathbf{e}_r}\langle \nabla w_\varepsilon\big|_{\Gamma_\xi}, \nabla w_\varepsilon\big|_{\Gamma_\xi}\rangle + 2\varepsilon dr_2 \langle \nabla dw[dr_2]\big|_\Gamma, \nabla w\big|_\Gamma\rangle + \mathcal{O}(\varepsilon^2).$$

Computing now $\lim_{\varepsilon\to 0}\{dJ(\Omega_\varepsilon)[dr_1] - dJ(\Omega)[dr_1]\}/\varepsilon$ proves (9) due to

$$\langle \nabla dw[dr_2]\big|_\Gamma, \nabla w\big|_\Gamma\rangle = \frac{\partial w}{\partial \mathbf{n}}\langle \nabla dw[dr_2]\big|_\Gamma, \mathbf{n}\rangle = \frac{\partial w}{\partial \mathbf{n}}\frac{\partial dw[dr_2]}{\partial \mathbf{n}}.$$

The homogeneous Dirichlet data $w|_\Gamma = 0$ imply the identity

$$(\|\nabla w\|^2)|_\Gamma = \left(\frac{\partial w}{\partial \mathbf{n}}\right)^2.$$

Moreover, observing $-\sqrt{r^2 + r'^2}\partial/\partial \mathbf{t} = \partial/\partial\phi$, we can decompose

$$\frac{\partial}{\partial \mathbf{e}_r}\left(\|\nabla w\|^2\right) = \frac{2}{\sqrt{r^2 + r'^2}}\frac{\partial w}{\partial \mathbf{n}}\left\{r\frac{\partial^2 w}{\partial \mathbf{n}^2} - r'\frac{\partial^2 w}{\partial \mathbf{n}\partial \mathbf{t}}\right\},$$

where $\partial^2 w/\partial^2 \mathbf{n} := \langle \nabla^2 w \cdot \mathbf{n}, \mathbf{n}\rangle$ and $\partial^2 w/(\partial \mathbf{n}\partial \mathbf{t}) := \langle \nabla^2 w \cdot \mathbf{n}, \mathbf{t}\rangle$. Since w is harmonical, admitting homogeneous Dirichlet data on Γ, we arrive at the identity

$$\frac{\partial^2 w}{\partial \mathbf{n}^2} = -\kappa\frac{\partial w}{\partial \mathbf{n}},$$

where κ denotes the curvature with respect to Γ, see Eppler and Harbrecht (2003b) for details. Hence, we can simplify (9) in accordance with (8). ■

3. Analyzing the shape Hessian

3.1. Boundary integral equations

In this subsection we compute the unknown boundary data of the state functions v and w by boundary integral equations. We introduce the single layer and the double layer operator with respect the boundaries $\Phi, \Psi \in \{\Gamma, \Sigma\}$ by

$$(V_{\Phi\Psi}u)(\mathbf{x}) := -\frac{1}{2\pi}\int_\Phi \log\|\mathbf{x} - \mathbf{y}\| u(\mathbf{y}) d\sigma_{\mathbf{y}}, \qquad \mathbf{x} \in \Psi,$$

$$(K_{\Phi\Psi}u)(\mathbf{x}) := \frac{1}{2\pi}\int_\Phi \frac{\langle \mathbf{x} - \mathbf{y}, \mathbf{n}_{\mathbf{y}}\rangle}{\|\mathbf{x} - \mathbf{y}\|^2} u(\mathbf{y}) d\sigma_{\mathbf{y}}, \qquad \mathbf{x} \in \Psi.$$

Note that $V_{\Phi\Psi}$ denotes an operator of order -1 if $\Phi = \Psi$, i.e. $V_{\Phi\Phi} : H^{-1/2}(\Phi) \to H^{1/2}(\Phi)$, while it is an arbitrarily smoothing compact operator if $\Phi \neq \Psi$ since

$\operatorname{dist}(\Gamma,\Sigma) > 0$. Likewise, if $\Sigma,\Gamma \in C^2$, the double layer operator $K_{\Phi\Phi} : H^{1/2}(\Phi) \to H^{1/2}(\Phi)$ is compact while it smoothes arbitrarily if $\Phi \neq \Psi$. We refer the reader to Hackbusch (1989), Kress (1989) for more details concerning boundary integral equations.

For the sake of simplicity we suppose that $\operatorname{diam}\Omega < 1$ to ensure that $V_{\Phi\Phi}$ is invertible, see Hsiao and Wendland (1977). Then, the normal derivative of w is given by the Dirichlet-to-Neumann map

$$\begin{bmatrix} V_{\Gamma\Gamma} & V_{\Sigma\Gamma} \\ V_{\Gamma\Sigma} & V_{\Sigma\Sigma} \end{bmatrix} \begin{bmatrix} \frac{\partial w}{\partial \mathbf{n}}\big|_\Gamma \\ \frac{\partial w}{\partial \mathbf{n}}\big|_\Sigma \end{bmatrix} = \begin{bmatrix} 1/2 + K_{\Gamma\Gamma} & K_{\Sigma\Gamma} \\ K_{\Gamma\Sigma} & 1/2 + K_{\Sigma\Sigma} \end{bmatrix} \begin{bmatrix} 0 \\ f \end{bmatrix}, \tag{10}$$

see (1). Likewise, the unknown boundary data of v are determined by

$$\begin{bmatrix} V_{\Gamma\Gamma} & -K_{\Sigma\Gamma} \\ -V_{\Gamma\Sigma} & 1/2 + K_{\Sigma\Sigma} \end{bmatrix} \begin{bmatrix} \frac{\partial v}{\partial \mathbf{n}}\big|_\Gamma \\ v|_\Sigma \end{bmatrix} = \begin{bmatrix} 1/2 + K_{\Gamma\Gamma} & -V_{\Sigma\Gamma} \\ -K_{\Gamma\Sigma} & V_{\Sigma\Sigma} \end{bmatrix} \begin{bmatrix} 0 \\ g \end{bmatrix}. \tag{11}$$

Note that here and in the sequel the operators $(1/2+K_{\Phi\Phi})$, $\Phi \in \{\Gamma,\Sigma\}$, have to be understood as continuous and bijective operators in terms of $(1/2 + K_{\Phi\Phi}) : H^{1/2}(\Phi)/\mathbb{R} \to H^{1/2}(\Phi)/\mathbb{R}$.

The unknown boundary data of the local shape derivatives $dv = dv[dr]$ and $dw = dw[dr]$ are derived by

$$\begin{bmatrix} V_{\Gamma\Gamma} & V_{\Sigma\Gamma} \\ V_{\Gamma\Sigma} & V_{\Sigma\Sigma} \end{bmatrix} \begin{bmatrix} \frac{\partial dw}{\partial \mathbf{n}}\big|_\Gamma \\ \frac{\partial dw}{\partial \mathbf{n}}\big|_\Sigma \end{bmatrix} = \begin{bmatrix} 1/2 + K_{\Gamma\Gamma} & K_{\Sigma\Gamma} \\ K_{\Gamma\Sigma} & 1/2 + K_{\Sigma\Sigma} \end{bmatrix} \begin{bmatrix} -\langle \mathbf{V}, \mathbf{n}\rangle \frac{\partial w}{\partial \mathbf{n}}\big|_\Gamma \\ 0 \end{bmatrix} \tag{12}$$

and

$$\begin{bmatrix} V_{\Gamma\Gamma} & -K_{\Sigma\Gamma} \\ -V_{\Gamma\Sigma} & 1/2 + K_{\Sigma\Sigma} \end{bmatrix} \begin{bmatrix} \frac{\partial dv}{\partial \mathbf{n}}\big|_\Gamma \\ dv|_\Sigma \end{bmatrix} = \begin{bmatrix} 1/2 + K_{\Gamma\Gamma} & -V_{\Sigma\Gamma} \\ -K_{\Gamma\Sigma} & V_{\Sigma\Sigma} \end{bmatrix} \begin{bmatrix} -\langle \mathbf{V}, \mathbf{n}\rangle \frac{\partial v}{\partial \mathbf{n}}\big|_\Gamma \\ 0 \end{bmatrix}. \tag{13}$$

3.2. Compactness of the Hessian at the optimal domain

Next, we will investigate the shape Hessian at the optimal domain $\Omega^\star$, that is, if the given inclusion is detected and the first order necessary condition (6) holds. Consequently, all quantities arising in the considerations are related to the optimal domain $\Omega^\star$ throughout this subsection. Since there holds $v = w$ in (1) at $\Omega^\star$, the first two terms in (8) vanish and the shape Hessian simplifies according to

$$d^2J(\Omega^\star)[dr_1, dr_2] = \int_0^{2\pi} 2\, dr_1\, r \frac{\partial v}{\partial \mathbf{n}} \left\{ \frac{\partial dw[dr_2]}{\partial \mathbf{n}} - \frac{\partial dv[dr_2]}{\partial \mathbf{n}} \right\} d\varphi. \tag{14}$$

LEMMA 3.1 *There holds*

$$\frac{\partial dw[dr]}{\partial \mathbf{n}} \equiv \frac{\partial dv[dr]}{\partial \mathbf{n}} \quad \text{on } \Gamma$$

if and only if the Dirichlet data of the local shape derivatives at Γ*, that is*

$$dv[dr] = dw[dr] = dr\frac{r}{\sqrt{r^2 + r'^2}}\frac{\partial v}{\partial \mathbf{n}} \quad \text{on } \Gamma,$$

are identical to zero. Moreover, $dw[dr] - dv[dr] \equiv const.$ *in* $\Omega^\star$ *holds only if* $const. = 0$*.*

Proof. The harmonic function $u := dw[dr] - dv[dr]$ satisfies the overdetermined boundary value problem

$$\begin{aligned} \Delta u &= 0 && \text{in } \Omega, \\ u &= 0 && \text{on } \Gamma, \\ u &= -dv[dr] && \text{on } \Sigma, \\ \frac{\partial u}{\partial \mathbf{n}} &= \frac{\partial dw[dr]}{\partial \mathbf{n}} && \text{on } \Sigma. \end{aligned}$$

The identity $u \equiv 0$ is equivalent to $dv[dr]|_\Sigma, (\partial dw[dr]/\partial \mathbf{n})|_\Sigma \equiv 0$. Hence, since $(\partial dv[dr]/\partial \mathbf{n})|_\Sigma, dw[dr]|_\Sigma \equiv 0$ due to the boundary conditions in (4), we conclude that $u \equiv 0$ is equivalent to $dv[dr], dw[dr] \equiv 0$. ∎

Integration by parts shows the identity

$$d^2J(\Omega^\star)[dr, dr] = \int_{\Omega^\star} \|\nabla(dv[dr] - dw[dr])\|^2 d\mathbf{x}.$$

Consequently, since nontrivial measurements $f, g \not\equiv 0$ imply $(\partial v/\partial \mathbf{n})|_\Gamma \not\equiv 0$, the above lemma leads immediately to

$$d^2J(\Omega^\star)[dr, dr] = \int_{\Omega^\star} \|\nabla(dv[dr] - dw[dr])\|^2 d\mathbf{x} > 0 \quad \text{for all } dr \not\equiv 0,$$

which means that the shape Hessian is positive. However, we emphasize that the domain $\Omega^\star$ is only a regular strict minimizer of second order if the shape Hessian is strict $H^{1/2}(\Gamma)$-coercive, that is $d^2J(\Omega^\star)[dr, dr] \geq c\|dr\|^2_{H^{1/2}(\Gamma)}$, see Dambrine and Pierre (2000), Dambrine (2002). We shall show next that strict $H^{1/2}(\Gamma)$-coercivity is not satisfied.

Lemma 3.2 *Let* (3) *hold, then the multiplication operator*

$$M : H^{1/2}(\Gamma) \to H^{1/2}(\Gamma), \qquad Mdr := dr \cdot \frac{r}{\sqrt{r^2 + r'^2}}\frac{\partial v}{\partial \mathbf{n}}\Big|_\Gamma \tag{15}$$

is continuous.

Proof. Abbreviating $u := r/\sqrt{r^2 + r'^2}(\partial v/\partial \mathbf{n})|_\Gamma$ we may write $Mdr = dr \cdot u$. Due to results of Triebel (1983) or Maz'ja and Shaposhnikova (1985), the multiplication operator M is continuous from $H^{1/2}(\Gamma)$ to $H^{1/2}(\Gamma)$, provided that $u \in C^{0,\alpha}(\Gamma)$ for some $\alpha > 1/2$. From (3) we conclude $u \in C^{1,\alpha}(\Gamma)$ which implies the assertion. ∎

LEMMA 3.3 *The operator associated with the difference of the Dirichlet-to-Neumann maps with respect to the Dirichlet data $h[dr] := Mdr$*

$$\Lambda : H^{1/2}(\Gamma) \to H^{-1/2}(\Gamma), \qquad \Lambda(h[dr]) := \frac{\partial dw[dr]}{\partial \mathbf{n}}\Big|_\Gamma - \frac{\partial dv[dr]}{\partial \mathbf{n}}\Big|_\Gamma. \tag{16}$$

is compact.

Proof. We deduce from (12) and (13) that

$$\begin{aligned}\left[V_{\Gamma\Gamma} - K_{\Sigma\Gamma}(1/2 + K_{\Sigma\Sigma})^{-1}V_{\Gamma\Sigma}\right] \frac{\partial dv}{\partial \mathbf{n}}\Big|_\Gamma &= \left[1/2 + K_{\Gamma\Gamma}\right. \\ &\quad \left. - K_{\Sigma\Gamma}(1/2 + K_{\Sigma\Sigma})^{-1}K_{\Gamma\Sigma}\right] h, \\ \left[V_{\Gamma\Gamma} - V_{\Sigma\Gamma}V_{\Sigma\Sigma}^{-1}V_{\Gamma\Sigma}\right] \frac{\partial dw}{\partial \mathbf{n}}\Big|_\Gamma &= \left[1/2 + K_{\Gamma\Gamma} - V_{\Sigma\Gamma}V_{\Sigma\Sigma}^{-1}K_{\Gamma\Sigma}\right] h.\end{aligned}$$

Since in both equations the operators on the left as well as on the right hand side are invertible and their difference is compact, we conclude

$$A\frac{\partial dv}{\partial \mathbf{n}}\Big|_\Gamma = Bh, \qquad [A + \mathcal{C}_1] \frac{\partial dw}{\partial \mathbf{n}}\Big|_\Gamma = [B + \mathcal{C}_2]\, h,$$

where A and B are bijective and continuous and $\mathcal{C}_1$ and $\mathcal{C}_2$ are compact perturbations in the associated spaces. Therefore we arrive at

$$\frac{\partial dw}{\partial \mathbf{n}}\Big|_\Gamma - \frac{\partial dv}{\partial \mathbf{n}}\Big|_\Gamma = \left[(A + \mathcal{C}_1)^{-1}(B + \mathcal{C}_2) - A^{-1}B\right] h$$

which is the desired result, since

$$(A + \mathcal{C}_1)^{-1}(B + \mathcal{C}_2) - A^{-1}B = (A + \mathcal{C}_1)^{-1}\mathcal{C}_2 + \left[(A + \mathcal{C}_1)^{-1} - A^{-1}\right] B$$

is compact. ∎

In order to illustrate the compact behaviour of the operator Λ we consider an analytic example concerning the situation of a ringshaped domain given by two concentric circles.

EXAMPLE 3.1 *Let $D = B_1(\mathbf{0}) \subset \mathbb{R}^2$ be the unit circle and $S = B_R(\mathbf{0})$ for some $0 < R < 1$. Then we have $\Omega = D \setminus S := \{(\rho, \varphi) : \rho \in (R, 1),\ \varphi \in [0, 2\pi)\}$, $\Sigma = \{(\rho, \varphi) : \rho = 1,\ \varphi \in [0, 2\pi)\}$, and $\Gamma = \{(\rho, \varphi) : \rho = R,\ \varphi \in [0, 2\pi)\}$. Harmonic*

functions on such ringshaped domains can be represented via an ansatz in polar coordinates

$$u(\rho,\varphi) = A_0 + B_0 \log\rho + \sum_{n=1}^{\infty} \left(A_n \rho^n + \frac{A_{-n}}{\rho^n} \right) \cos n\varphi + \left(B_n \rho^n + \frac{B_{-n}}{\rho^n} \right) \sin n\varphi.$$

Expanding the Dirichlet data $h = dv|_\Gamma = dw|_\Gamma$ *in a Fourier series*

$$h = h_0 + \sum_{n=1}^{\infty} h_n \cos n\varphi + h_{-n} \sin n\varphi,$$

and observing the boundary condition $dw|_\Sigma = 0$*, we arrive at*

$$dw(\rho,\varphi) = h_0 \frac{\log\rho}{\log R} + \sum_{n=1}^{\infty} \frac{R^n}{1-R^{2n}} \left(\frac{1}{\rho^n} - \rho^n \right) (h_n \cos n\varphi + h_{-n} \sin n\varphi).$$

Similarly, from $(\partial dv/\partial \mathbf{n})|_\Sigma = (\partial dv/\partial\rho)|_{\rho=1} = 0$*, we conclude that*

$$dv(\rho,\varphi) = h_0 + \sum_{n=1}^{\infty} \frac{R^n}{1+R^{2n}} \left(\frac{1}{\rho^n} + \rho^n \right) (h_n \cos n\varphi + h_{-n} \sin n\varphi).$$

Employing $(\partial dw/\partial \mathbf{n})|_\Gamma = -(\partial dw/\partial\rho)|_{\rho=R}$ *and likewise for* dv*, we find that*

$$\frac{\partial dw}{\partial \mathbf{n}}\Big|_\Gamma - \frac{\partial dv}{\partial \mathbf{n}}\Big|_\Gamma = \frac{h_0}{R\log R} - 4\sum_{n=1}^{\infty} \frac{nR^{2n-1}}{1-R^{4n}} (h_n \cos n\varphi + h_{-n} \sin n\varphi).$$

The exponential decay of the resulting Fourier coefficients clearly indicates the compactness of the map Λ*. Moreover, the decay is the faster the smaller the radius* R *of the inclusion.*

Obviously (14) defines a continuous bilinear form on $H^{1/2}(\Gamma) \times H^{1/2}(\Gamma)$, namely

$$d^2 J(\Omega^\star)[dr_1, dr_2] = \langle 2M dr_1, \Lambda(M dr_2) \rangle, \tag{17}$$

where $\langle \cdot, \cdot \rangle$ denotes the canonical $L^2(\Gamma)$-inner product. According to the Lemmas 3.2 and 3.3 we conclude the final result.

PROPOSITION 3.1 *The shape Hessian*

$$H : H^{1/2}(\Gamma) \to H^{-1/2}(\Gamma), \qquad H = 2M^\star \Lambda M : H^{1/2}(\Gamma) \to H^{-1/2}(\Gamma),$$

is compact at the optimal domain $\Omega^\star$*.*

This proposition implies the ill-posedness of the optimization problem itself, which is completely characterized by the nature of the shape Hessian at the critical domain. However, our considerations specify no detailed information on the eigenvalues of the shape Hessian. If Γ is analytical the eigenvalues of the shape Hessian decrease *exponentially*. This issues from the fact that the boundary integral operators, which transfer the data from Σ to Γ, are arbitrarily smooth. Hence, $(\partial v/\partial \mathbf{n})|_\Gamma$ is analytical, even though $g \in H^{-1/2}(\Sigma)$, and the multiplication operator $M : H^s(\Gamma) \to H^s(\Gamma)$ becomes continuous for any $s \in \mathbb{R}$. Since $\Lambda : H^{-s}(\Gamma) \to H^s(\Gamma)$ is compact for any $s \in \mathbb{R}$, strict $H^s(\Gamma)$-coercivity of any finite order is *not* satisfied for the problem under consideration. Therefore, the exponential ill-posedness of the inverse problem is completely reflected by the shape Hessian at the optimal domain $\Omega^\star$.

We will illustrate this exponential ill-posedness by two examples. The first example given below is computed analytically. The second one, concerned with the constellation of Fig. 1, is presented in Section 5, where we compute the eigenvalues numerically.

EXAMPLE 3.2 *We consider the same configuration as in Example 3.1, i.e.,* $\Omega = \{(\rho,\varphi) : \rho \in (R,1),\ \varphi \in [0,2\pi)\}$. *If we choose for example the Dirichlet data* $f := (x^2-y^2)|_{\rho=1} = \cos 2\varphi$ *we conclude* $g = 2(1+R^4)/(1-R^4)\cos\varphi$ *and* $(\partial v/\partial \mathbf{n})|_\Gamma = (\partial w/\partial \mathbf{n})|_\Gamma = -4R/(1-R^4)\cos\varphi$. *Straightforward calculation leads to*

$$d^2J(\Omega^\star)[\cos k\varphi,\cos l\varphi] = d^2J(\Omega^\star)[\sin k\varphi,\sin l\varphi]$$
$$= \begin{cases} \frac{32R^4\pi}{(1-R^4)^2}\left[\frac{(k-2)R^{2k-4}}{1-R^{4k-8}} + \frac{(k+2)R^{2k+4}}{1-R^{4k+8}}\right], & \text{if } k=l>2,\\ \frac{32R^4\pi}{(1-R^4)^2}\frac{(k+2)R^{2k+4}}{1-R^{4k+8}}, & \text{if } |k-l|=4 \text{ and } k,l>2,\\ 0, & \text{if } |k-l|\neq 0,4 \text{ and } k,l>2. \end{cases}$$

and $d^2J(\Omega^\star)[\cos k\varphi,\sin l\varphi] = 0$ *for all* $k,l>2$. *Consequently, the shape Hessian is a banded matrix with coefficients exhibiting an exponential decay with respect to higher frequencies.*

Despite the fact that we have not introduced any finite dimensional approximation of the minimization problem yet, we have to keep in mind *exponentially* growing condition numbers of the discrete shape Hessian when increasing the degrees of freedom. However, the shape Hessian consists of two well-posed parts, namely the parts associated with v and w. Consequently, the numerical approximation of its coefficients is not affected by this degeneration and only governed by the discretization error of the boundary element method.

4. Discretization

4.1. Finite dimensional approximation of boundaries

Since the infinite dimensional optimization problem cannot be solved directly, we replace it by a finite dimensional problem. Based on polar coordinates, we can express the smooth function $r \in C^{2,\alpha}_{\mathrm{per}}([0,2\pi])$ by the Fourier series

$$r(\phi) = a_0 + \sum_{n=1}^{\infty} a_n \cos n\phi + a_{-n} \sin n\phi.$$

Hence, it is reasonable to approximate the radial function by a truncated Fourier series

$$r_{N_r}(\phi) = a_0 + \sum_{n=1}^{N_r} a_n \cos n\phi + a_{-n} \sin n\phi. \tag{18}$$

If r is analytical, the Fourier series r_{N_r} converges to r exponentially in N_r, which means that r_{N_r} is a p-approximation of r.

Since r_{N_r} admits $2N_r+1$ degrees of freedom $a_{-N_r}, a_{1-N_r}, \ldots, a_{N_r}$, we arrive at a finite dimensional optimization problem in the open set

$$A_{N_r} := \{a_{-N_r}, a_{1-N_r}, \ldots, a_{N_r} \in \mathbb{R} : r_{N_r}(\phi) > 0,\ \phi \in [0,2\pi]\} \subset \mathbb{R}^{2N_r+1}.$$

Hence, via the identification $r_{N_r} \Leftrightarrow \Omega_{N_r}$, the finite dimensional approximation of shape minimization problem (2) reads as

$$J(\Omega_{N_r}) \to \min\,. \tag{19}$$

The associated gradients and Hessians have to be computed with respect to all directions $dr, dr_1, dr_2 = \cos N_r\phi, \cos(N_r-1)\phi, \ldots, \sin(N_r-1)\phi, \sin N_r\phi$.

4.2. Treating the optimization problem

The minimization problem defined by (19) implies finding of its stationary points $\Omega^{\star}_{N_r}$

$$dJ(\Omega^{\star}_{N_r})[dr] = 0 \tag{20}$$

for all directions $dr \in \{\cos N_r\phi, \cos(N_r-1)\phi, \ldots, \sin(N_r-1)\phi, \sin N_r\phi\}$.

To solve (20), we consider on the one hand a method which is based only on first order information, namely a quasi Newton method updated by the inverse BFGS-rule without damping, see Gill, Murray and Wright (1982), and Grossman and Terno (1993) for details.

On the other hand, we perform a Newton method which we regularize since the shape Hessian is compact at the optimal domain $\Omega^{\star}$. Namely, abbreviating

the discrete gradient by $\mathbf{G}_n$ and the associated Hessian by $\mathbf{H}_n$, we consider in the n-th iteration step the descent direction

$$\mathbf{h}_n := -(\mathbf{H}_n^2 + \alpha_n \mathbf{I})^{-1} \mathbf{H}_n \mathbf{G}_n,$$

where $\alpha_n > 0$ is an appropriately chosen regularization parameter. This descent direction $\mathbf{h}_n$ solves the minimization problem

$$\|\mathbf{H}_n \mathbf{h}_n - \mathbf{G}_n\|^2 + \alpha_n \|\mathbf{h}_n\|^2 \to \min$$

and corresponds to a Tikhinov regularization of equation (20). Moreover, note that we employ in both methods a quadratic line search with respect to the functional (2).

4.3. Numerical method to compute the state

Given the formulas (2), (7) and (8), the functional, its gradient as well as its Hessian can be computed from the knowledge of the boundary data of the state equations (1) and (4). These data are given by the boundary integral equations (10)–(13). Hence, it is rather convenient to employ a boundary element method to compute the required boundary data of the state equations. We use a Galerkin discretization by N_Φ piecewise linear functions $\{\theta_i^\Phi\}_{i=1}^{N_\Phi}$ on each boundary $\Phi \in \{\Sigma, \Gamma\}$. For $\Phi, \Psi \in \{\Sigma, \Gamma\}$, we introduce the system matrices

$$\mathbf{V}_{\Phi\Psi} = -\frac{1}{2\pi} \left[\int_\Psi \int_\Phi \log \|\mathbf{x} - \mathbf{y}\| \theta_i^\Phi(\mathbf{y}) \theta_j^\Psi(\mathbf{x}) d\sigma_\mathbf{y} d\sigma_\mathbf{x} \right]_{i=1,\dots,N_\Phi,\, j=1,\dots,N_\Psi},$$

$$\mathbf{K}_{\Phi\Psi} = \frac{1}{2\pi} \left[\int_\Psi \int_\Phi \frac{\langle \mathbf{x} - \mathbf{y}, \mathbf{n}_\mathbf{y} \rangle}{\|\mathbf{x} - \mathbf{y}\|^2} \theta_i^\Phi(\mathbf{y}) \theta_j^\Psi(\mathbf{x}) d\sigma_\mathbf{y} d\sigma_\mathbf{x} \right]_{i=1,\dots,N_\Phi,\, j=1,\dots,N_\Psi},$$

and the mass matrices

$$\mathbf{M}_\Phi = \left[\int_\Phi \theta_i^\Phi(\mathbf{x}) \theta_j^\Phi(\mathbf{x}) d\sigma_\mathbf{x} \right]_{i,j=1,\dots,N_\Phi},$$

and the load vectors of Dirichlet data f_Φ and Neumann data g_Φ

$$\mathbf{f}_\Phi = \left[\int_\Phi \theta_i^\Phi(\mathbf{x}) f(\mathbf{x}) d\sigma_\mathbf{x} \right]_{i=1,\dots,N_\Phi}, \qquad \mathbf{g}_\Phi = \left[\int_\Phi \theta_i^\Phi(\mathbf{x}) g(\mathbf{x}) d\sigma_\mathbf{x} \right]_{i=1,\dots,N_\Phi}.$$

Then, the linear system of equations

$$\begin{bmatrix} \mathbf{V}_{\Gamma\Gamma} & \mathbf{V}_{\Sigma\Gamma} \\ \mathbf{V}_{\Gamma\Sigma} & \mathbf{V}_{\Sigma\Sigma} \end{bmatrix} \begin{bmatrix} \mathbf{a}_\Gamma \\ \mathbf{a}_\Sigma \end{bmatrix} = \begin{bmatrix} 1/2\mathbf{M}_\Gamma + \mathbf{K}_{\Gamma\Gamma} & \mathbf{K}_{\Sigma\Gamma} \\ \mathbf{K}_{\Gamma\Sigma} & 1/2\mathbf{M}_\Sigma + \mathbf{K}_{\Sigma\Sigma} \end{bmatrix} \begin{bmatrix} \mathbf{M}_\Gamma^{-1} \mathbf{f}_\Gamma \\ \mathbf{M}_\Sigma^{-1} \mathbf{f}_\Sigma \end{bmatrix}, \quad (21)$$

gives us the Neumann data $a_\Gamma = \sum_{i=1}^{N_\Gamma} [\mathbf{a}_\Gamma]_i \theta_i^\Gamma$ on Γ and $a_\Sigma = \sum_{i=1}^{N_\Sigma} [\mathbf{a}_\Sigma]_i \theta_i^\Sigma$ on Σ from the Dirichlet data on Γ and Σ. Likewise, the system

$$\begin{bmatrix} \mathbf{V}_{\Gamma\Gamma} & -\mathbf{K}_{\Sigma\Gamma} \\ -\mathbf{V}_{\Gamma\Sigma} & 1/2\mathbf{M}_\Sigma + \mathbf{K}_{\Sigma\Sigma} \end{bmatrix} \begin{bmatrix} \mathbf{b}_\Gamma \\ \mathbf{a}_\Gamma \end{bmatrix} = \begin{bmatrix} 1/2\mathbf{M}_\Gamma + \mathbf{K}_{\Gamma\Gamma} & -\mathbf{V}_{\Sigma\Gamma} \\ -\mathbf{K}_{\Gamma\Sigma} & \mathbf{V}_{\Sigma\Sigma} \end{bmatrix} \begin{bmatrix} \mathbf{M}_\Gamma^{-1} \mathbf{g}_\Gamma \\ \mathbf{M}_\Sigma^{-1} \mathbf{f}_\Sigma \end{bmatrix}, \quad (22)$$

yields the Dirichlet data $b_\Gamma = \sum_{i=1}^{N_\Gamma} [\mathbf{b}_\Gamma]_i \theta_i^\Gamma$ on Γ and the Neumann data $a_\Sigma = \sum_{i=1}^{N_\Sigma} [\mathbf{a}_\Sigma]_i \theta_i^\Sigma$ on Σ from the Neumann data $\mathbf{g}_\Gamma$ on Γ and the Dirichlet data $\mathbf{f}_\Sigma$ on Σ.

Observing that

$$\frac{\partial}{\partial \phi} \frac{\partial v}{\partial \mathbf{n}} = -\frac{1}{\sqrt{r^2 + r'^2}} \frac{\partial^2 v}{\partial \mathbf{n} \partial \mathbf{t}} \quad \text{on } \Gamma$$

due to homogeneous Dirichlet conditions at Γ, the variables $\left(\partial^2 v/(\partial \mathbf{n} \partial \mathbf{t})\right)\big|_\Gamma$ and likewise $\left(\partial^2 w/(\partial \mathbf{n} \partial \mathbf{t})\right)\big|_\Gamma$, required for the shape Hessian, can be computed by differentiating the piecewise linear representations of $(\partial v/\partial \mathbf{n})|_\Gamma$ and $(\partial w/\partial \mathbf{n})|_\Gamma$, respectively.

We mention that the appearing system matrices have to be computed only once for each domain while the systems (21) and (22) have to be solved very often with different right hand sides to obtain the local shape derivatives. Hence, we recommend to use a *wavelet Galerkin scheme* which yields quasi sparse system matrices. We refer to Eppler and Harbrecht (2003a, b, c, d) for more details on the wavelet based fast solution of boundary integral equations appearing in shape optimization.

5. Numerical results

5.1. Quasi Newton versus regularized Newton method

In our first example we consider the situation depicted in Fig. 1, i.e., we choose the ellipse with semiaxes 0.45 and 0.3 as the domain D. The inclusion centered in $\mathbf{x} = (0, 0)^T$ is described by 15 Fourier coefficients. The Dirichlet data on $\Sigma = \partial D$ are chosen as $f = (x^2 - y^2)|_\Sigma$ while the Neumann data g on Σ are computed numerically with high accuracy.

The Hessian $d^2 J(\Omega^\star)[dr_1, dr_2]$ discretized via 65 Fourier coefficients ($N_r = 32$) is visualized in Fig. 2. A plot of its eigenvalue distribution can be found in Fig. 3. We mention that the first 16 eigenvalues are smaller than zero which results from numerical roundoff errors, even though we applied $N_\Gamma = N_\Sigma = 1024$ boundary elements. The plot exhibits clearly the exponential decay of the eigenvalues. The ℓ^2-condition number of the discrete Hessian is about 10^9.

We employ the circle of radius 0.25 indicated by the dashed line in Fig. 4 as the initial guess in our regularized Newton method. It turns out that setting $\alpha_n = 2^{-n}$ in the n-th step of the regularized Newton method is the best choice of the regularization parameter. Thus, in each step we reduce the regularization parameter by the factor of 2. We observe that, similarly to multiscale methods, in the first steps the low frequencies of the boundary are approximated while the high frequencies are increasingly resolved during the iteration. Let us mention that the line search prevents the divergence of the method, particularly in the last iteration steps. The dash-dotted line in the right plot of Fig. 4 indicates

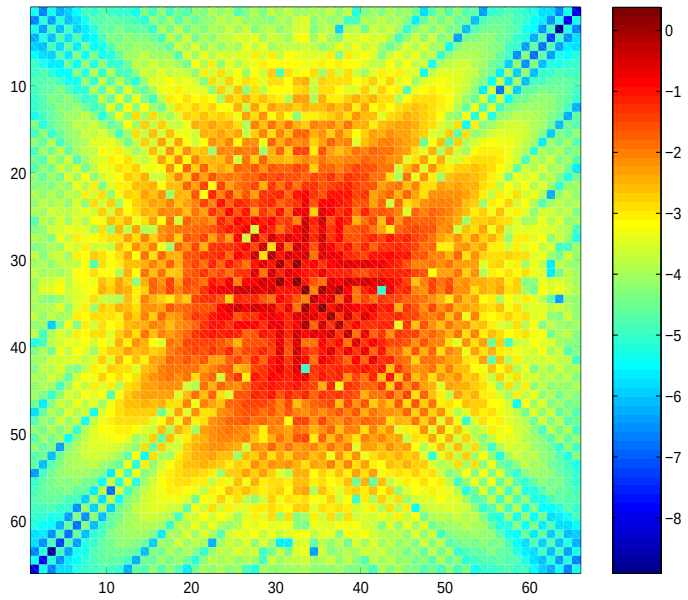

Figure 2. Logarithmic moduli of the coefficients of the discrete Hessian $d^2J(\Omega^\star)[dr_1, dr_2]$.

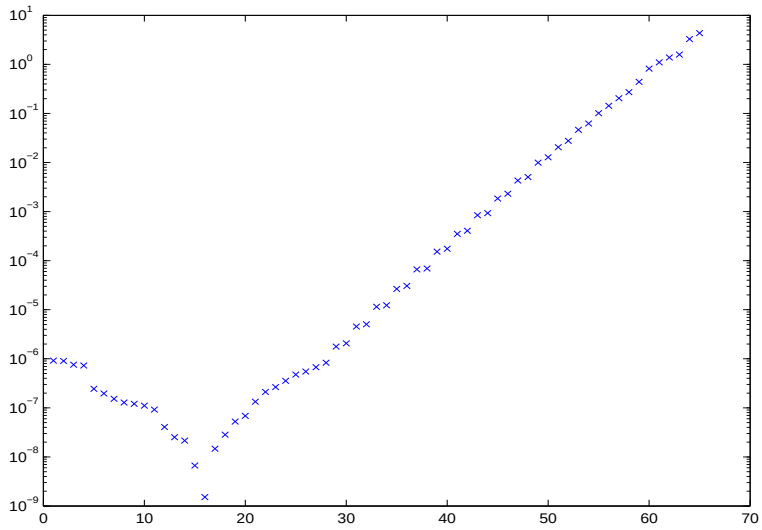

Figure 3. The eigenvalues of the discrete Hessian.

the solution in the case of 33 Fourier coefficients ($N_r = 16$) obtained after 50 steps of the regularized Newton method using 512 boundary elements on each boundary ($N_\Gamma = N_\Sigma = 512$). The right plot contains the solution after 50 steps of the quasi Newton method.

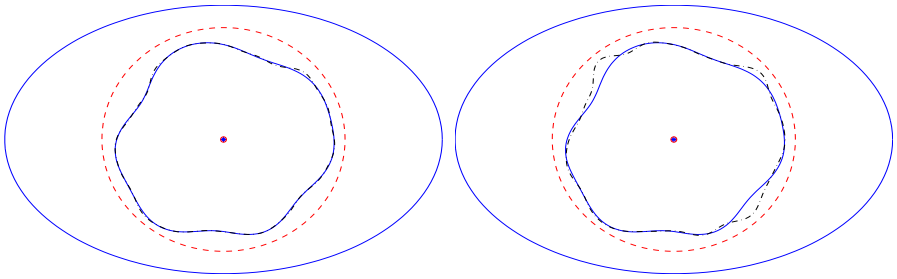

Figure 4. Initial guess and final approximation of the inclusion for 33 Fourier coefficients in case of the regularized Newton method (left) and the quasi Newton method (right).

The progress of the minimization of the shape functional during the iteration and the corresponding shape approximation errors measured by the ℓ^2-norm of the Fourier coefficients are plotted in Fig. 5. The solid and dashed lines correspond to the regularized Newton and quasi Newton method, respectively. One observes faster convergence and higher accuracy for the regularized Newton scheme. In particular, one recognizes from the plot concerning the functional that the objective is $2.8 \cdot 10^{-3}$ in the case of the initial guess and $3.5 \cdot 10^{-11}$ in the last step.

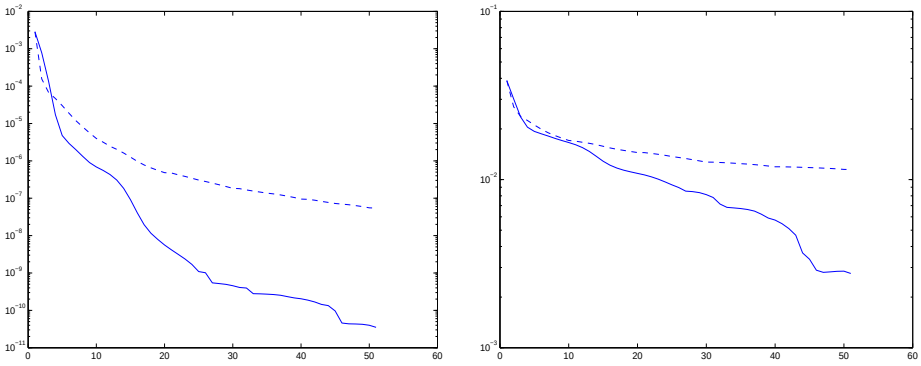

Figure 5. The values of the shape functional (left) and the ℓ^2-norm of the shape approximation errors (right).

Figs. 4 and 5 confirm that the regularized Newton method computes the given inclusion more exactly than the quasi Newton method.

5.2. Preprocessing: Detecting the barycentre

To apply the shape calculus from Subsection 2.2 for a refined resolution of the interface, the position of the pole of the polar coordinate system has to be detected in advance. To our experience the determination of this pole should be combined with a first crude predetermination of the shape of the given inclusion.

From the general formula (5), for a constant shift field $\mathbf{V} \equiv \mathbf{a}$ we derive the directional derivatives

$$dJ[\mathbf{a}] = \int_\Gamma \langle \mathbf{a}, \mathbf{n} \rangle \left[\left(\frac{\partial v}{\partial \mathbf{n}} \right)^2 - \left(\frac{\partial w}{\partial \mathbf{n}} \right)^2 \right] d\sigma = \left\langle \mathbf{a}, \int_\Gamma \mathbf{n} \left[\left(\frac{\partial v}{\partial \mathbf{n}} \right)^2 - \left(\frac{\partial w}{\partial \mathbf{n}} \right)^2 \right] d\sigma \right\rangle .$$

Based on these directional derivatives, the implementation of a first order optimization algorithm is straightforward.

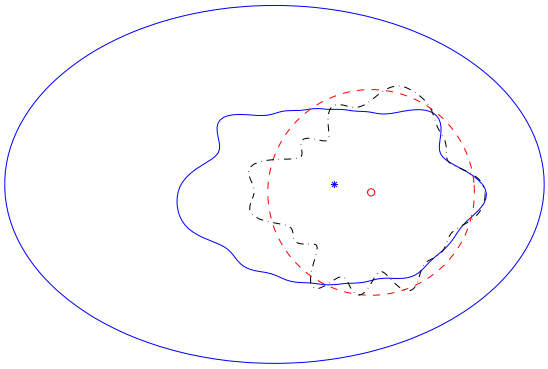

Figure 6. Approximation of the inclusion for the best fitting ball.

We choose the same setup as in the first example but consider a lengthy inclusion centered in $\mathbf{x} = (0.1, 0)$, see Fig. 6. The preprocessing step performed with the best fitting circle does not yield satisfying results since the circle is placed too close to the right boundary, see Fig. 6 (dashed line). Neither first nor second order optimization methods detect the left boundary if this circle is used as initial guess for a refined resolution of the boundary (dash-dotted line).

Hence, we should consider more degrees of freedom with respect to the boundary. To ensure that the pole is equal to the barycentre, the radial function shall fulfill $r(\varphi) = r(\varphi + \pi)$. In our experience, the best choice to get a crude approximation of the shape is the use of periodic cubic splines. We subdivide the interval $[0, 2\pi)$ equidistantly into eight intervals and denote the smoothest

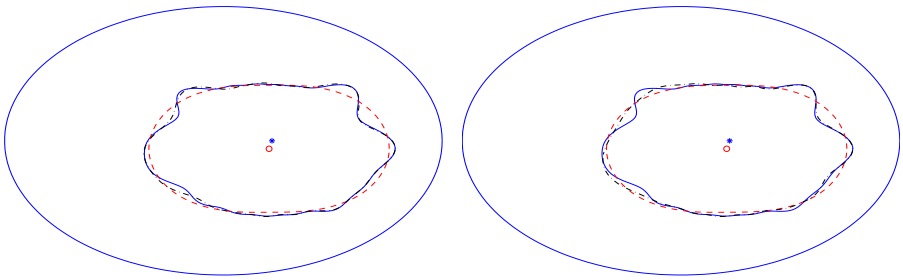

Figure 7. Preprocessing using B-splines and final approximation using the regularized Newton method (left) and the quasi Newton method (right).

n-th 2π-periodic cardinal B-spline of order three on the given partitioning by B_n^3. The ansatz $r(\varphi) = \sum_{n=1}^{8} b_n B_n^3(\phi)$ yields the conditions $b_n = b_{n+4}$ to ensure $r(\varphi) = r(\varphi+\pi)$. Hence, we have to consider the four directions $dr = B_n^3 + B_{n+4}^3$ in addition to the shift fields $\mathbf{a} = [1,0]^T, [0,1]^T$. These are six degrees of freedom which we minimized in the preprocessing step. The result of this preprocessing is indicated by the dashed line in Fig. 7.

The final approximation via 33 Fourier coefficients and 30 iterations of the regularized Newton method is presented in the left plot Fig. 7. The plot on the right hand side shows the final approximation in case of 50 quasi Newton iterations. Again, the regularized Newton method resolves the inclusion more exactly, particularly the left part of its boundary. We remark that after the 45th iteration step of the regularized Newton method the ℓ^2-condition number of the Hessian is greater than 10^{16}.

In both calculations, the preprocessing has been performed by 30 iteration steps of a quasi Newton method updated by the inverse BFGS-rule without damping, where the initial guess has been the circle of radius 0.1 and midpoint $(0,0)$. We mention that only a few boundary elements are required for the preprocessing. In fact, we chose $N_\Gamma = N_\Sigma = 64$. For the refined resolution of the boundary we set $\alpha_n = 2^{-n}$ and $N_\Gamma = N_\Sigma = 512$.

5.3. Scaling the inclusion

In our last example we employ again the setup of the previous subsections but consider different scaled inclusions centered in $(-0.1, -0.05)$. The preprocessing is performed like above by using B-splines and 30 quasi Newton iterations. We iterate 30 times the regularized Newton scheme setting $\alpha_n = 2^{-n}$ and $N_\Gamma = N_\Sigma = 512$. The solutions are presented in Fig. 8. As these plots confirm, the resolution of the boundary seems to be the more inexact the smaller the inclusion. Nevertheless, the results confirm the stability of the regularized Newton method.

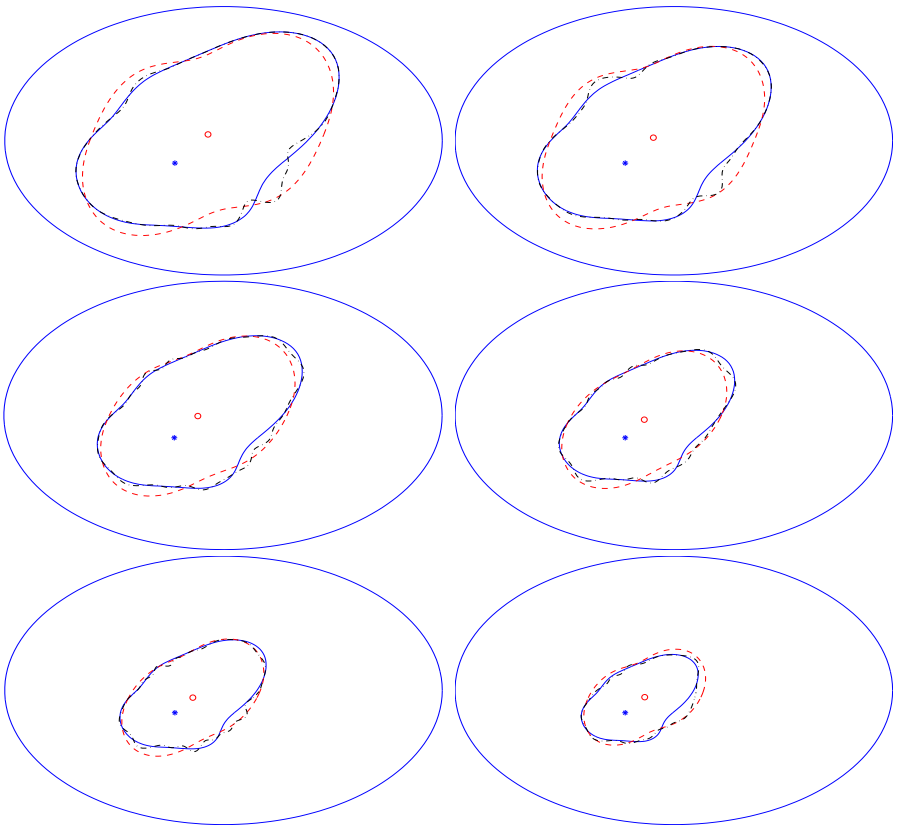

Figure 8. Preprocessing and final approximation by the regularized Newton method while reducing the size of the inclusion.

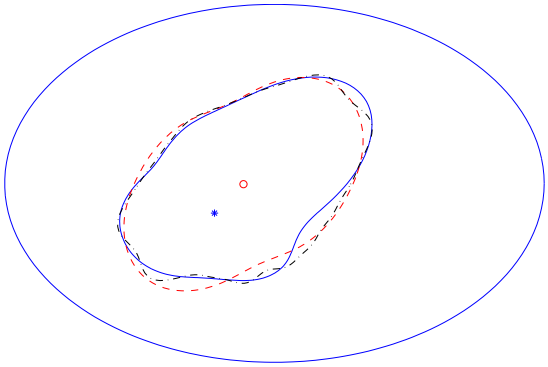

Figure 9. Approximation of the inclusion by the quasi Newton method.

Compared to the solution of the quasi Newton method, the resolution of the inclusion is more precise. For example, in Fig. 9, the solution obtained after 50 steps of the quasi Newton method is depicted. It corresponds to the right hand plot in the middle of Fig. 8.

6. Conclusion

The present paper is concerned with the second order methods for the identification of voids or inclusions. The problem under consideration is well known to be severely ill-posed. Since the shape Hessian is compact at the optimal domain, we propose a regularized Newton method for the resolution of the inclusion. Combined with a preprocessing step to detect the barycentre and a first crude approximation of the inclusion, the numerical results evince that the regularized Newton method resolves the given inclusion more exactly than the first order methods.

Acknowledgement

We are deeply grateful to Dr. Andreas Rathsfeld for valuable discussions and several helpful comments.

References

Akduman, I. and Kress, R. (2002) Electrostatic imaging via conformal mapping. *Inverse Problems* **18**, 1659–1672.

Alessandrini, G., Isakov, V. and Powell, J. (1995) Local uniqueness in the inverse problem with one measurement. *Trans. Am. Math. Soc.* **347**, 3031–3041.

Brühl, M. (2001) Explicit characterization of inclusions in electrical impedance tomography. *SIAM J. Math. Anal.* **32** (6), 1327–1341.

Brühl, M. and Hanke, M. (2000) Numerical implementation of two noniterative methods for locating inclusions by impedance tomography. *Inverse Problems* **16** (4), 1029–1042.

Chapko, R. and Kress, R. (2003) A hybrid method for inverse boundary value problems in potential theory To appear.

Dambrine, M. and Pierre, M. (2000) About stability of equilibrium shapes. *M2AN* **34** (4), 811–834.

Dambrine, M. (2000) Hessiennes de forme et stabilite des formes critiques. PhD Thesis, Ecole Normale Superieure de Cachan.

Dambrine, M. (2002) On variations of the shape Hessian and sufficient conditions for the stability of critical shapes. *RACSAM, Rev. R. Acad. Cien. Serie A. Mat.* **96** (1), 95–121.

Delfour, M. and Zolesio, J.-P. (2001) *Shapes and Geometries*. SIAM, Philadelphia.

Eppler, K. (2000) Optimal shape design for elliptic equations via BIE-methods. *J. of Applied Mathematics and Computer Science* **10**, 487–516,

Eppler, K. (2000) Boundary integral representations of second derivatives in shape optimization. *Discussiones Mathematicae (Differential Inclusion Control and Optimization)* **20**, 63–78.

Eppler, K. and Harbrecht, H. (2003a) Numerical solution of elliptic shape optimization problems using wavelet-based BEM. *Optim. Methods Softw.* **18**, 105–123.

Eppler, K. and Harbrecht, H. (2003b) 2nd Order Shape Optimization using Wavelet BEM. *Preprint 06-2003, TU Berlin.* To appear in *Optim. Methods Softw.*

Eppler, K. and Harbrecht, H. (2003c) Exterior Electromagnetic Shaping using Wavelet BEM. *Preprint 13-2003, TU Berlin.* To appear in *Math. Meth. Appl. Sci.*

Eppler, K. and Harbrecht, H. (2003d) Fast wavelet BEM for 3d electromagnetic shaping. *Bericht 03-9*, Berichtsreihe des Mathematischen Seminars der Christian-Albrechts-Universitt zu Kiel. To appear in *Appl. Numer. Math.*

Eppler, K. and Harbrecht, H. (2004a) Shape optimization for 3D electrical impedance tomography. *Preprint 963, WIAS Berlin.* Submitted for publication.

Eppler, K. and Harbrecht, H. (2004b) Efficient Treatment of Stationary Free Boundary Problems. *Preprint 965, WIAS Berlin.* Submitted for publication.

Friedman, A. and Isakov, V. (1989) On the uniqueness in the inverse conductivity problem with one measurement. *Indiana Univ. Math. J.* **38**, 563–579.

Fujii, N. and Goto, Y. (1990) Second order numerical method for domain optimization problems. *Journal of Optimization Theory and Applications* **67** (3), 533–550.

Gill, P.E., Murray, W. and Wright, M.H. (1981) *Practical Optimization.* Academic Press, New York.

Grossmann, Ch. and Terno, J. (1993) *Numerik der Optimierung.* Teubner, Stuttgart.

Hackbusch, W. (1989) *Integralgleichungen.* B.G. Teubner, Stuttgart.

Hettlich, F. and Rundell, W. (1998) The determination of a discontinuity in a conductivity from a single boundary measurement. *Inverse Problems* **14**, 67–82.

Hsiao, G. and Wendland, W. (1977) A finite element method for some equations of first kind. *J. Math. Anal. Appl.* **58**, 449–481.

Novruzi, A. and Roche, J.-R. (1995) Second derivatives, Newton method, application to shape optimization. *INRIA-report* No. 2555.

Novruzi, A. (1997) Contribution en Optimisation des Formes et Applications. PHD Thesis, Nancy.

Novruzi, A. and Roche, J.-R. (2000) Newton Method in 3-dimensional shape optimization problems. Application to electromagnetic casting. *BIT* **40** (1), 102–120.

Kress, R. (1989) *Linear Integral Equations.* Springer-Verlag, Berlin-Heidelberg.

Maz'ya, V.G. and Shaposhnikova, T.O. (1985) *Theory of multipliers in spaces of differentiable functions.* Pitman, Boston. *Monographs and Studies in Mathematics* **23**. Pitman Advanced Publishing Program. Boston - London - Melbourne: Pitman Publishing Inc. *XIII*.

Roche, J.-R. and Sokolowski, J. (1996) Numerical methods for shape identification problems. *Control Cybern.* **25**, 867–894.

Sokolowski, J. and Zolesio, J.-P. (1992) *Introduction to Shape Optimization.* Springer, Berlin.

Triebel, H. (1983) *Theory of Function Spaces.* Birkhäuser, Basel-Boston-Stuttgart.